Subtask 3.1D

Hybrid Fractal Flame Model for SI Engine Combustion

Kazuie Nishiwaki

Takayuki Nakayama

Ritsumeikan University

Background

- Models for Turbulent Propagating Flame
  - Flamelet Models

    Fractal Flame Model

$$\overline{\omega} = \rho_u S_t \left|\nabla \overline{c}\right| \; ; \quad S_t / S_\lambda = \left(\varepsilon_i / \varepsilon_o\right)^{2-D}$$

$\overline{\omega}$: mean burning rate, ρ_u : density of reactants

S_t : turbulent flame velocity, S_λ : laminar flame velocity

$\left(\varepsilon_i / \varepsilon_o\right)^{2-D}$: fractal area, D : fractal dimension

ε_i : inner cutoff, ε_o : outer cutoff, $\overline{c}$: mean progress variable

Coherent Flame Model

$$\overline{\omega} = \rho_u S_l \Sigma$$

Σ : flame surface density

Motivation of the Study

- Problems posed for flamelet models
- Fractal Flame Model

$$S_t / S_\lambda = (\varepsilon_i / \varepsilon_o)^{2-D} \quad (1)$$

Fractal area and S_t/S_l :
Gülder et al.,
Comb. Flame, Vol. 120,
2000

Eq. (1) is not always valid

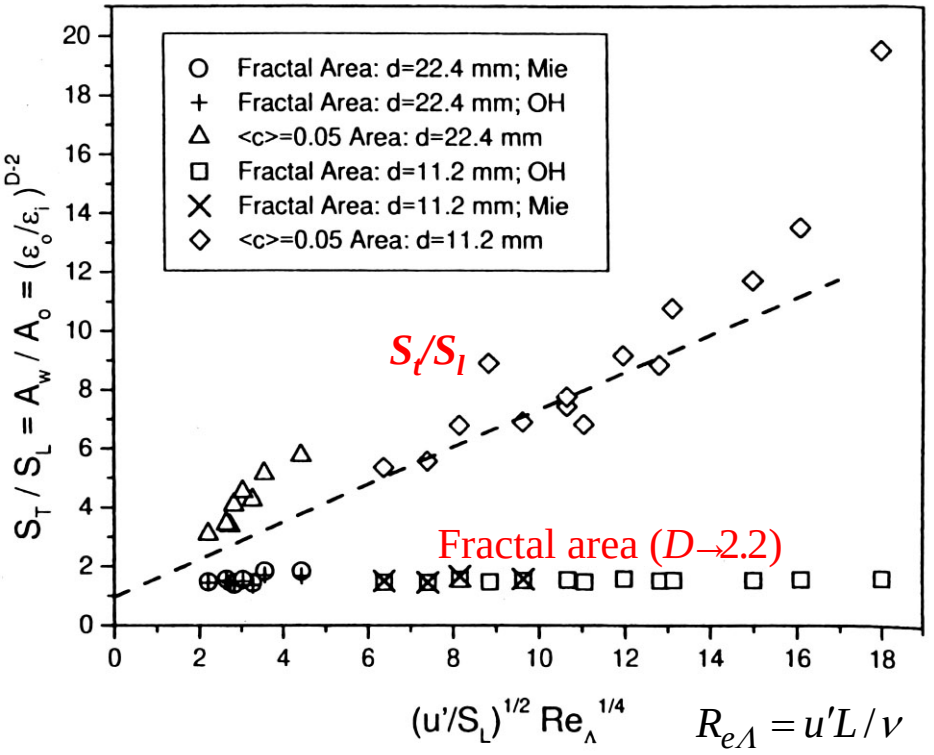

Motivation of the Study, cont'd

- Coherent Flame Model

$$\overline{\omega} = \rho_u S_l \Sigma$$

Flame surface density measurement in an engine by Smallwood et al., SAE 962088

Σ does not change much as engine speed changes

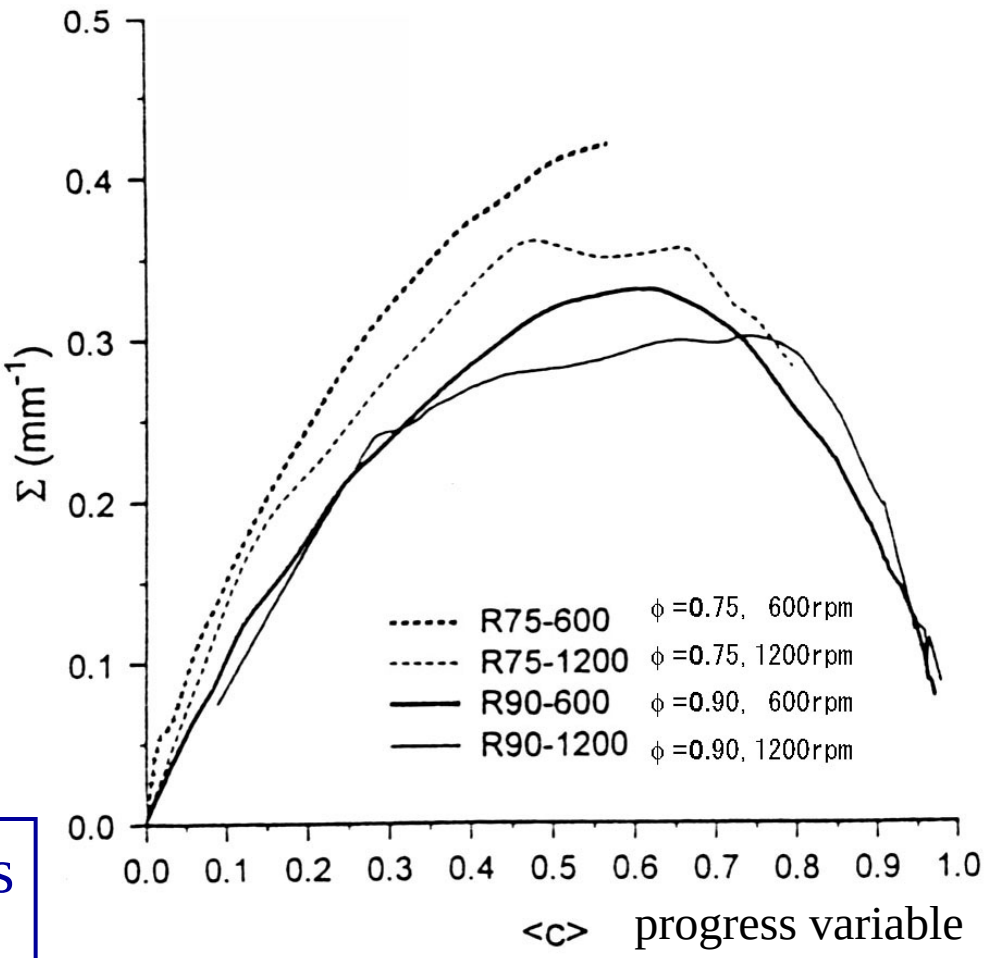

These two experimental evidences imply that the flamelets are not always laminar

Concept of Hybrid Fractal Flame Model

- The intermittency of turbulence
- Turbulent dissipation eddies are not continuous in a 3-dimensional field, but continuous in a D_T - dimensional field.
  (D_T is different from D of a wrinkled surface)
- The volume ratio, γ_K, of the eddies in Kolmogorov length scale:

$$\gamma_K = \left(\frac{\lambda_K}{\lambda} \right)^{3-D_T}$$

λ_K : Kolmogorov length scale

λ : length scale of most energetic eddies

D_T : fractal dimension expressing intermittency of turbulence

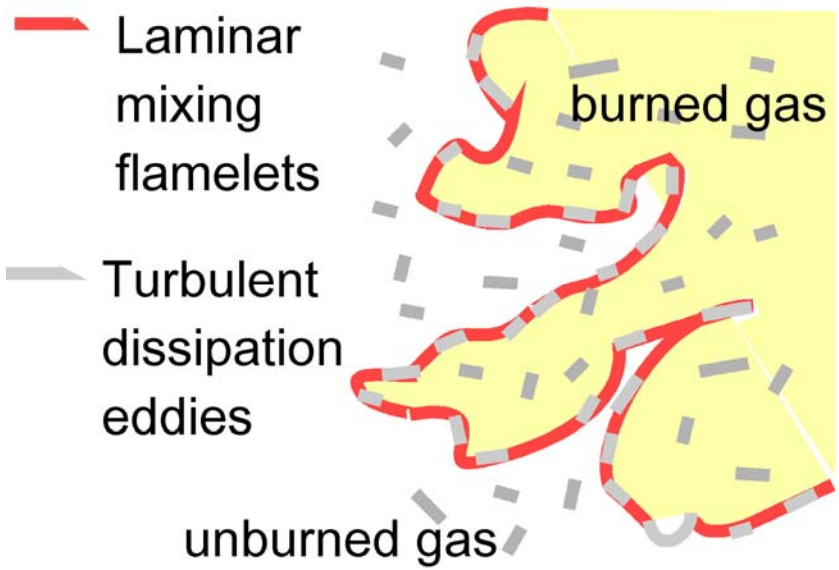

Formulation of Hybrid Fractal Flame Model

- Assumption: the flame is composed of turbulent dissipation flamelets and laminar mixing flamelets.

- The mean burning rate:

$$\overline{\omega} = \overline{\omega}_T \gamma_K + \overline{\omega}_L (1-\gamma_K) \quad ; \quad \begin{cases} \overline{\omega}_T = \rho_u \dfrac{1}{\tau_K} \overline{c}(1-\overline{c})\, f_W \\ \overline{\omega}_L = \rho_u S_T \left|\nabla \overline{c}\right| \end{cases}$$

[turbulent] [laminar]

ρ_u : density of unburned gas, τ_K : Kolmogorov time scale

$\overline{c}$: mean progress variable, S_T : turbulent flame speed

f_W : model function for wall effect(≤ 1)

Formulation of Turbulence Dissipation Flamelets

- Basic equations to solve for D_T, τ_K and λ/λ_K
- Turbulence energy spectrum function:

$$k = \alpha^* \int_{\kappa_0}^{\kappa_d} E(\kappa) d\kappa \quad ; E(\kappa) = \varepsilon^{2/3} \kappa^{-5/3} F(\kappa) \quad ; \kappa_0 = 1/\lambda ; \kappa_d = 1/\lambda_K$$

- The turbulence energy dissipation rate:

$$\varepsilon = 2\nu \int_{\kappa_0}^{\kappa_d} \alpha^* \kappa^2 E(\kappa) d\kappa$$

- The spatial average of ε_κ to the power p for the wave number κ:

$$\overline{\varepsilon_\kappa^p} = \varepsilon^p (\lambda\kappa)^{(p-1)(3-D_T)} \quad ; \quad p = 2/3$$

- The k -ε – l relationship:

$$\varepsilon = C' k^{3/2} / \lambda$$

$$C' = 0.201\left(1 + 5.30 R_t^{-1/2}\right)^{3/2} : \text{Makita's model} \quad ; \quad R_t = k^2/(\varepsilon\nu)$$

Formulation of Turbulence Dissipation Flamelets – cont'd

- Turbulence dissipation flamelets
- Fractal theory of intermittency of turbulence gives:

$$D_T = D_T^{\,*} F_D \qquad \begin{cases} D_T^{*} = 5 - 1.03\alpha^{*}\left(1 + 5.30 R_t^{-1/2}\right), \alpha^{*} = 2.27 \\ F_D = 1 + 1/\left(2.61 R_t^{0.276} - 5\right) \quad ; \quad R_t = k^2/(\varepsilon\nu) \end{cases}$$

$$1/\tau_K = \left(\varepsilon/\nu\right)^{1/2}\left(\lambda_K/\lambda\right)^{(3-D_T)/2}$$

$$\lambda_K/\lambda = L^{*} F_L \qquad \begin{cases} L^{*} = \left[6\alpha^{*}/\left\{(1+D_T)C'^{4/3} R_t\right\}\right]^{3/(1+D_T)} \\ F_L = \left(0.199 R_t^{0.805} - 2.19\right)/\left(0.199 R_t^{0.805} - 1.19\right) \end{cases}$$

$$C' = 0.201\left(1 + 5.30 R_t^{-1/2}\right)^{3/2}$$

Formulation of Laminar Mixing Flamelets

Fractal flame model:

- $S_t / S_\lambda = (\varepsilon_i / \varepsilon_o)^{2-D_L}$; ε_i : inner cutoff, ε_o : outer cutoff

- Model for D_L : Fractal Dimension Growth Model(FDGM)
  Suzuki and Nishiwaki, SAE 2004-01-1994

$$\frac{dD_2}{dt} = -\frac{1}{\tau}\{D_2 - D_{2\infty}\}$$

$$D_{2\infty} = f(u'/S_L, p/p_0)$$

$$\tau = g(u'/S_L, p/p_0)$$

$$D_L = D_2 + 1$$

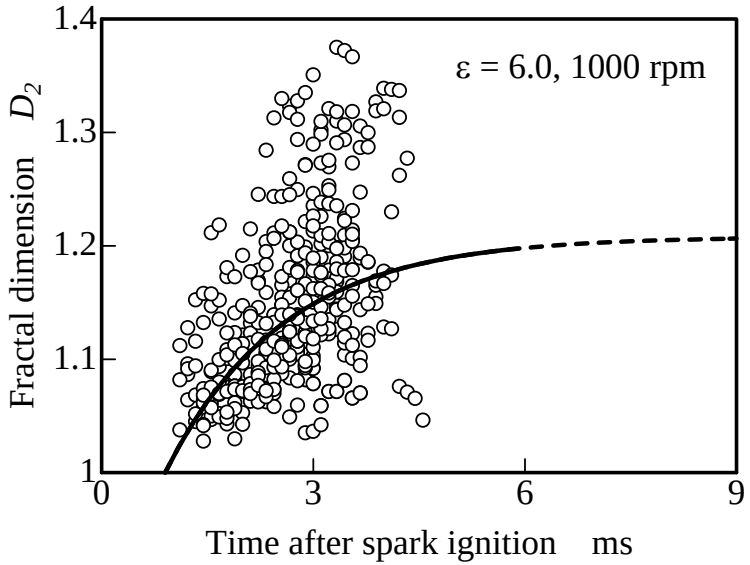

Computational Results and Comparison with Measurements

Test Engines and Operating Conditions

[Engine A]

Bore x Stroke : 86.0 x 84.0 mm
Comp. Ratio : 7.9
Fuel : Regular gasoline

Engine speed	Excess air ratio	Ignition time
1000 rpm	1.05	13 ˚btdc
1500	0.997	14
1800	0.957	20

[Engine B]

Bore x Stroke : 82.6 x 114.3 mm
Comp. Ratio : 7.0
Fuel : Iso-octane

Engine speed	Excess air ratio	Ignition time
750 rpm	1.0	15 ˚btdc
750	1.1	16
750	1.2	19

Combustion Models to Compare with Measurements

- $\overline{R}_{fu} = C_{\text{model}}\overline{\omega}(y_{fu,u} - y_{fu,b})$
  - HFFM(Hybrid Fractal Flame model)

    $\overline{\omega} = \overline{\omega}_T \gamma_K + \overline{\omega}_L (1-\gamma_K)$

  - FDGM(Fractal Dimension Growth model, pure fractal flame model)

    $\overline{\omega} = \overline{\omega}_L \quad (\gamma_K = 0)$

- The models are integrated into a CFD code.
  - The governing equations includes the general conservation equations in the Reynolds averaged form for mass, momentum, average enthalpy, enthalpy of unburned gas, progress variable, turbulence kinetic energy and its dissipation rate.

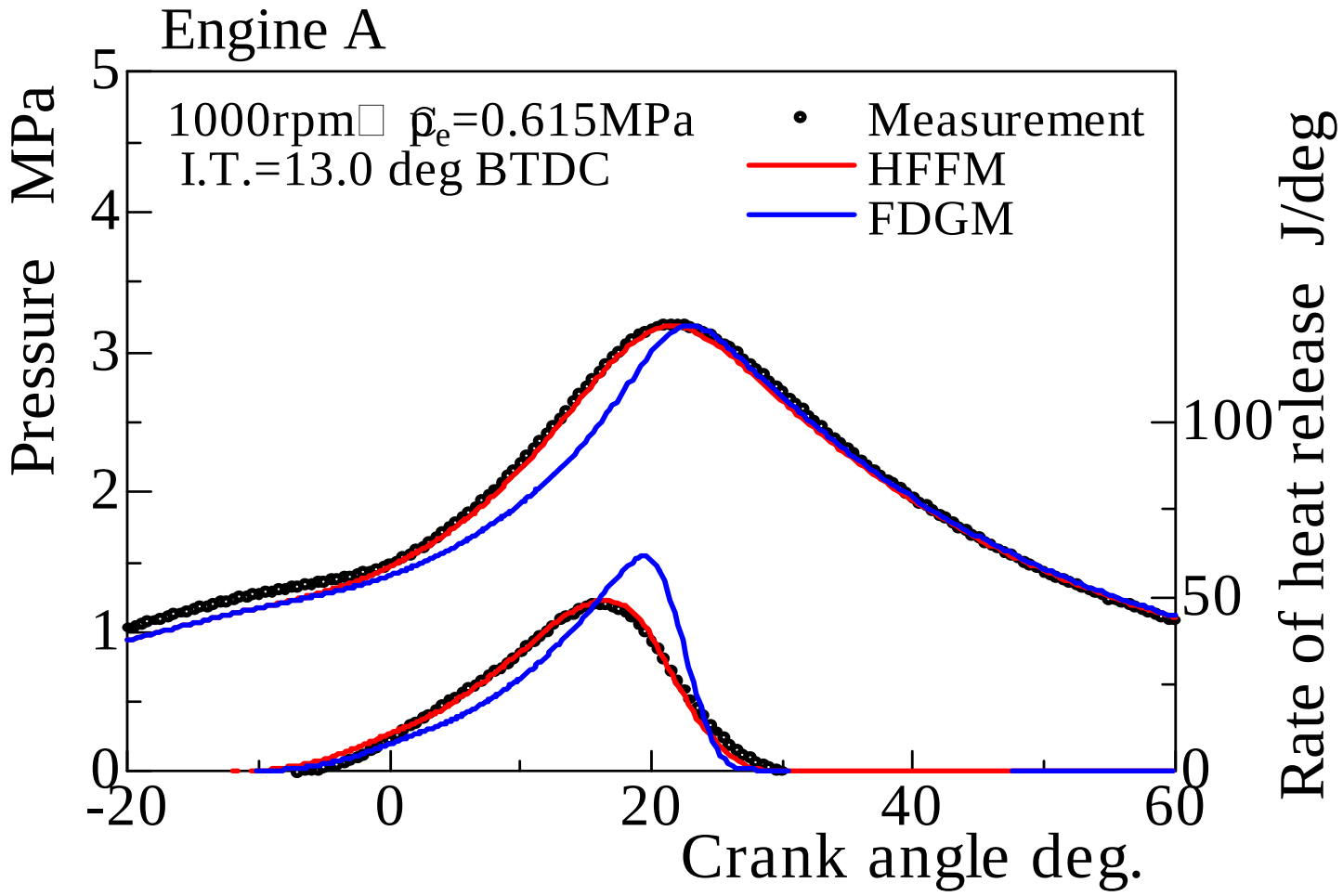

Adjustment of C_{model} to make the best fit to measured pressure at 1000 rpm for each model; C_{model} =2.95 for HFFM, C_{model} =2.60 for FDGM

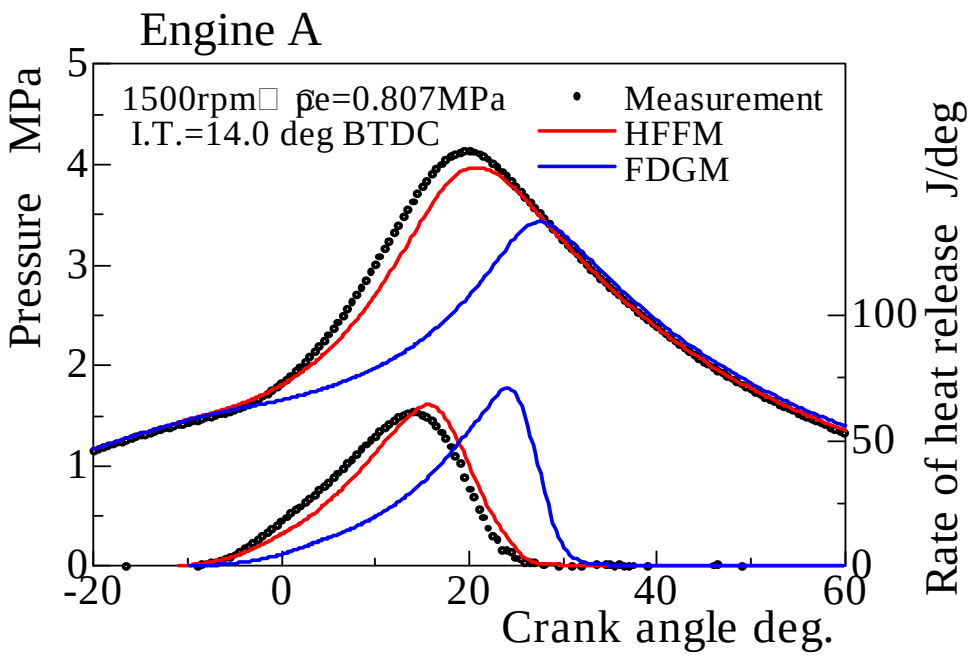

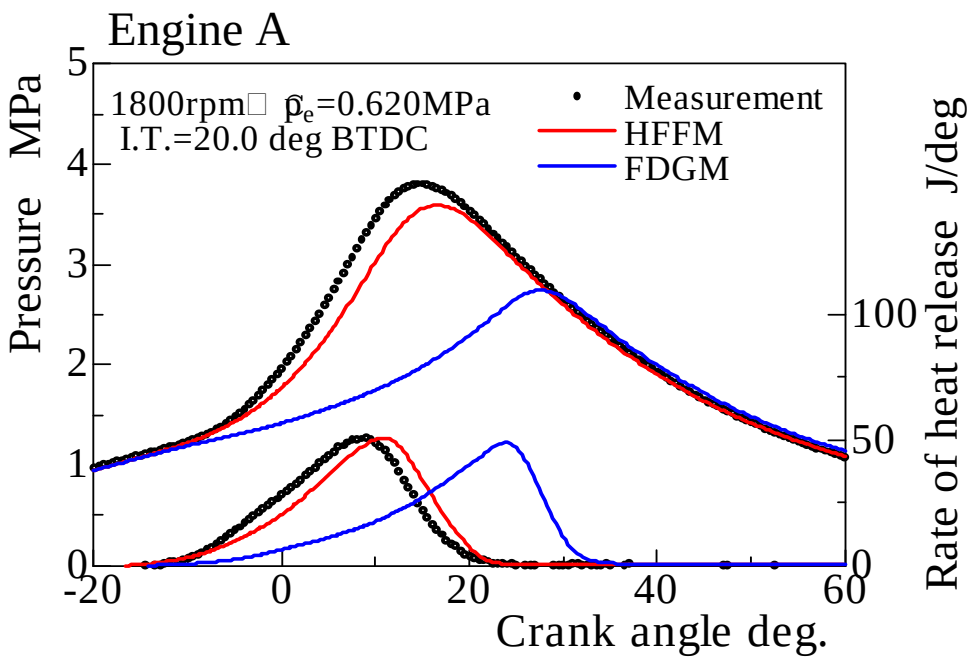

Comparison of computational results using same C_{model} as that for 1000 rpm with measurements for 1500 and 1800 rpm

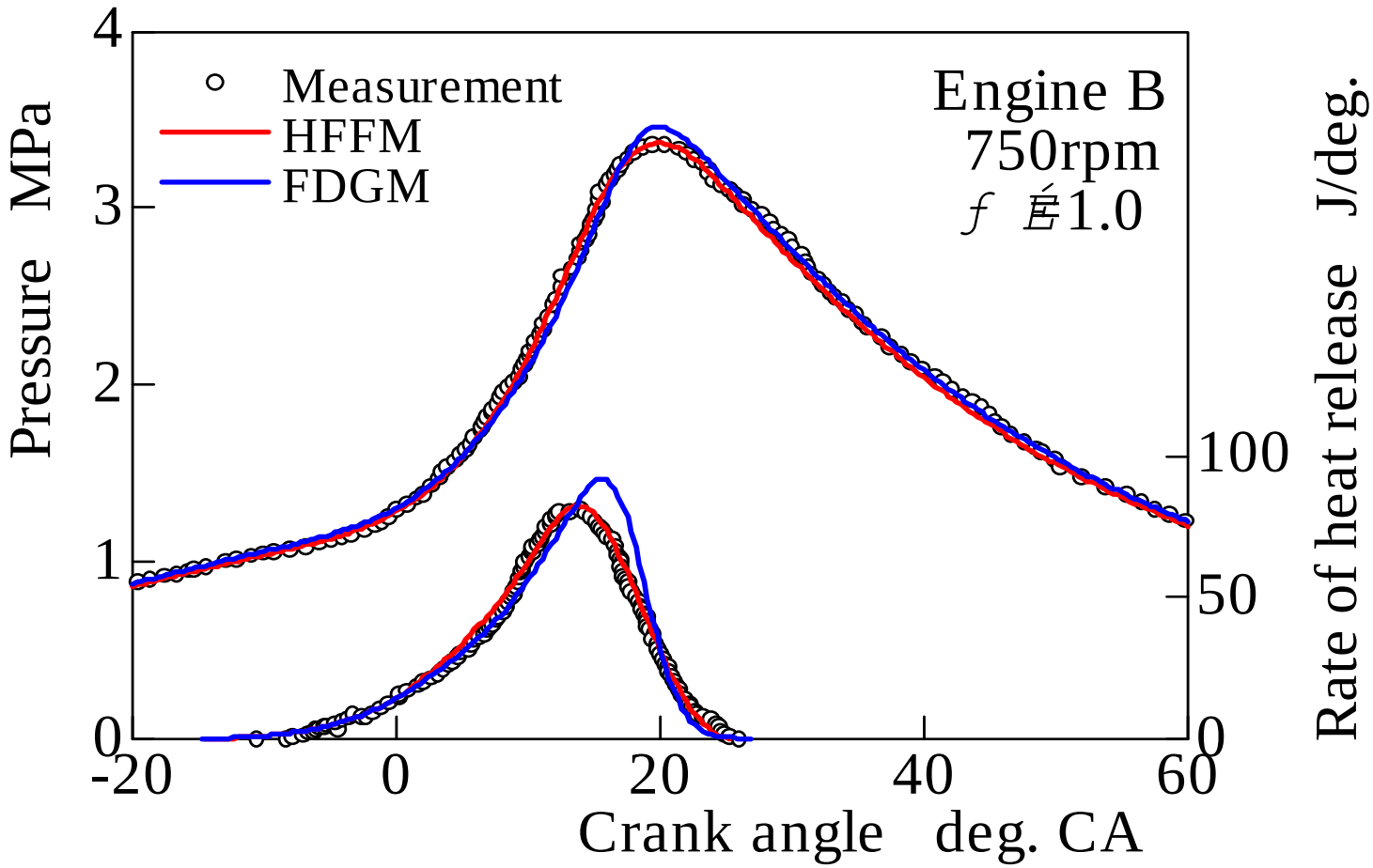

Adjustment of C_{model} of each model to measured pressure for λ=1.0

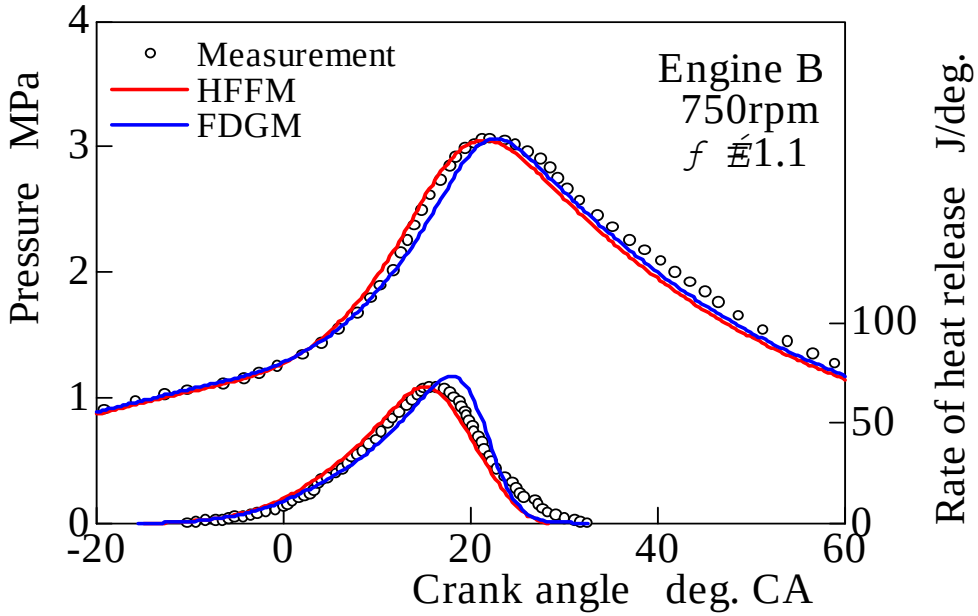

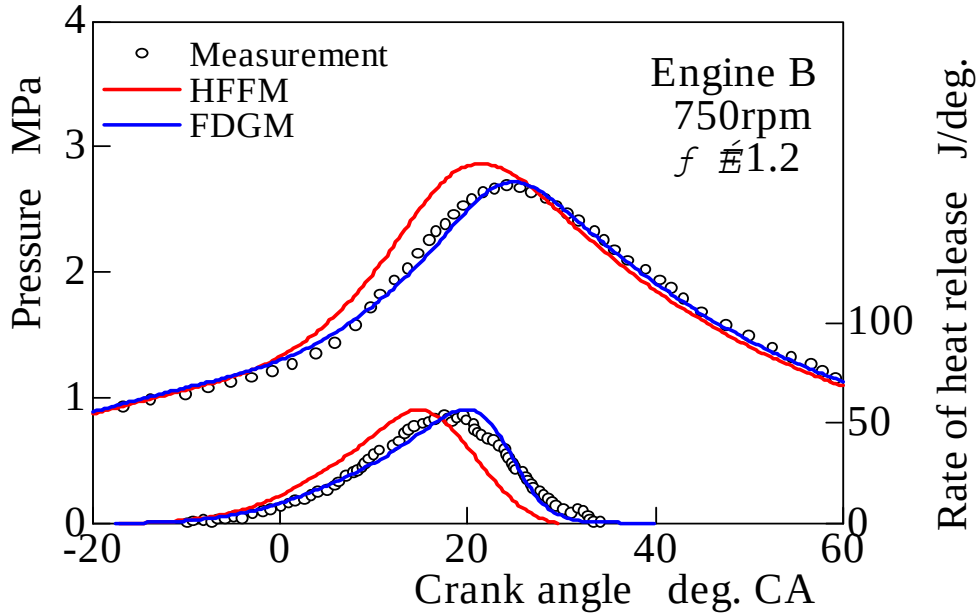

Comparison of computational results using same C_{model} as that for ϕ =1.0 with measurements for λ=1.1 and λ=1.2

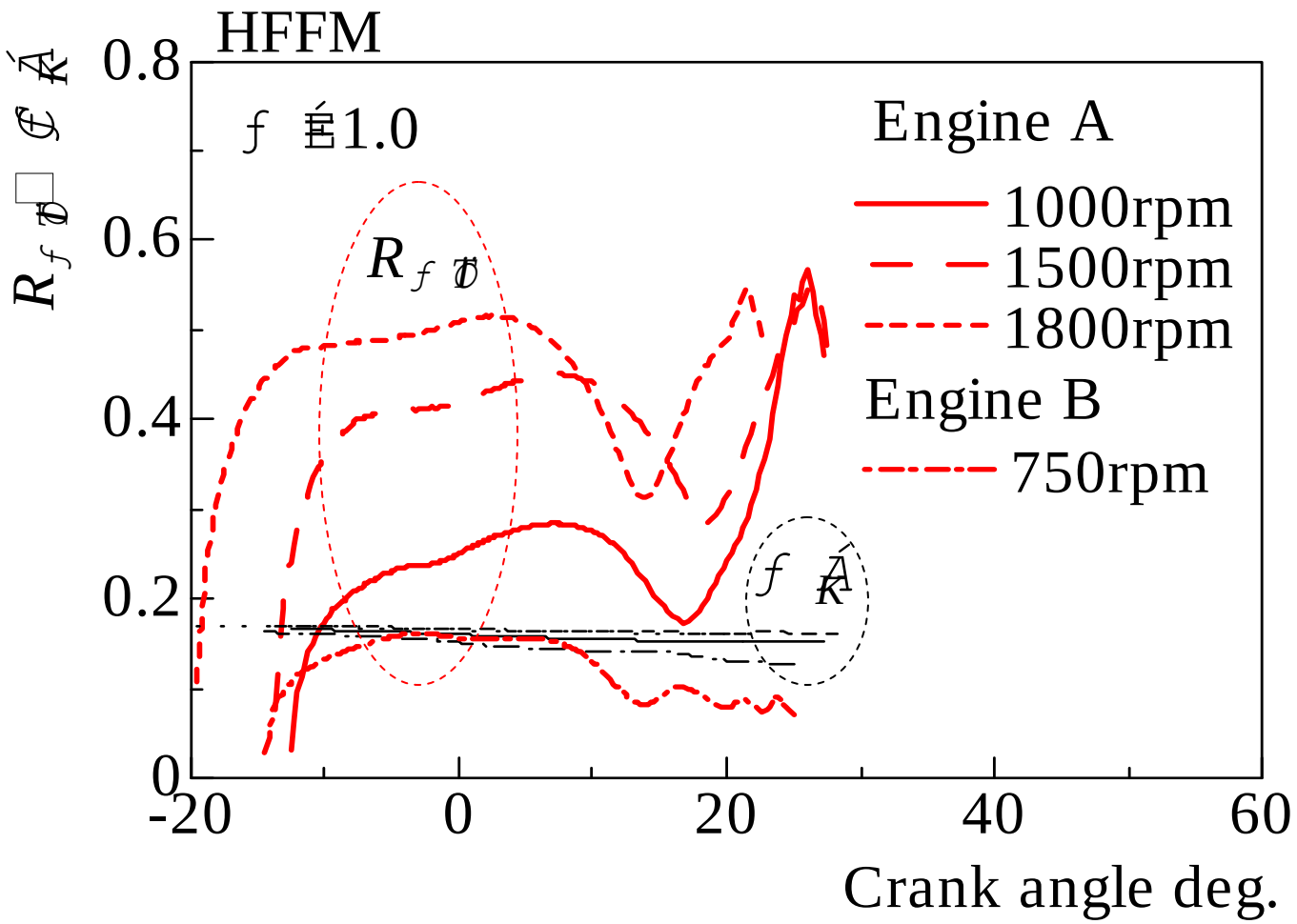

Contribution of Turbulent dissipation flamelet; HFFM ; Engine A and B

$R_{\omega T} = \omega_T \gamma_k / [\omega_T \gamma_K + \omega_L ((1-\gamma_K))]$

Conclusion

- The Hybrid Fractal Flame Model has been introduced for the prediction of SI engine combustion. The concept of the model is that the flame front consists of the laminar mixing flamelet and turbulent dissipation flamelet.

- The HFFM is much better than the laminar fractal flame model in predicting pressure for different engine speeds.

- The analysis of the computed results shows that the flame relies more on turbulent dissipation as the engine speed increases.

Proceedings of the Twenty-Ninth IEA/TLM, September, 2-6, 2007,Gembloux, Belgium

Hybrid Fractal Flame Model for SI Engine Combustion

Subtask 3.1D

Kazuie Nishiwaki and Takayuki Nakayama
Research Organization of Science and Engineering, Ritsumeikan University
1-1-1 Noji-Higashi, Kusatsu, Shiga 525-8577, Japan
E-mail: nswk@fc.ritsumei.ac.jp

ABSTRACT

A new combustion model has been introduced for the prediction of turbulent propagating combustion in SI engines. The model assumes that the flamelets consist of a turbulent dissipation part and a laminar part and is called Hybrid Fractal Flame Model (HFFM). A CFD code integrated the model and separately a pure laminar flamelet model, which was tested for comparison. Computational results were compared with measured pressures and heat release rates for different engine speeds. It is shown that the HFFM agrees well with the measurements for 1000, 1500 and 1800 rpm, whereas the laminar flamelet model underestimates as engine speed increases. The analysis of the computed results indicates that the turbulent dissipation heat release rate occupies a larger part of the total heat release rate as the engine speed increases; from around 20% at 1000 rpm to 50% at 1800 rpm.

INTRODUCTION

For the prediction of the combustion process in SI engines, several different combustion models have been evolved, which were derived from quite different concepts from each other. These models were categorized into the groups of a laminar flamelet concept and a turbulent dissipation concept. Comparisons of either type of the model with experiments, however, have not always been satisfactory. Gülder et al. (1) posed a fundamental problem with a fractal flame model, which belongs to a laminar flamelet model, showing the experimental results that the fractal flame area of the turbulent premixed flame becomes nearly constant and the fractal dimension stays 2.2 when turbulence intensity exceeds a certain value, whereas turbulent burning velocity still increases as the turbulence intensity increases. Smallwood et al. (2) presented the measurements of the flame surface density in an SI engine. They showed that the flame surface density has little variation over the range of engine speed investigated. These two experimental evidences imply that the flamelets, which make up a wrinkled flame front surface, are not always laminar.

The purpose of this study is to develop a new model that combines the laminar mixing and turbulent dissipation concept. The computed results are compared with measured data for several different equivalence ratios and engine speeds.

HYBRID FRACTAL FLAME MODEL (HFFM)

The fractal theory, on which the intermittency of turbulence is based, derives the volume ratio, γ_K , of the eddies in Kolmogorov length scale, ℓ_K , to the eddies in the most energetic length scale, ℓ , as follows:

$$\gamma_K = \left(\ell_K / \ell\right)^{3-D_T} \qquad \cdots\cdots\cdots\cdots\cdots\cdots (1)$$

where D_T is the fractal dimension expressing the intermittency of turbulence. The turbulent energy dissipates in this limited volume, which exists without regard to burned or unburned gas. The local combustion, which takes place in this volume, can be assumed to be dissipation-controlled, because the reaction rate is usually much higher than the turbulence dissipation rate; the Kolmogorov time scale in this study is between 10^{-4} s and 10^{-3} s, while the reaction time of hot flame reaction is on the order of 10^{-5} s.

It can be naturally assumed that the rest of the volume, 1-γ_K , is filled with turbulent eddies in the scales larger than Kolmogorov scale, in which the turbulent motion does not dissipate and transfers the turbulence energy from large scale eddies to small scale eddies. When burned and unburned eddies meet each other in this region, the local combustion can be assumed to be laminar.

To summarize, the model is composed of two different kinds of flamelet: the turbulent dissipation flamelet in

Kolmogorov scale and the laminar flamelet in scales larger than Kolmogorov scale.

The mean burning rate, $\overline{\omega}$, is composed of the burning rate due to the turbulent dissipation, $\overline{\omega}_T$, and that due to laminar mixing, $\overline{\omega}_L$, and is expressed in the form as

$$\overline{\omega} = \overline{\omega}_T \gamma_K + \overline{\omega}_L (1-\gamma_K) \quad \cdots\cdots(2)$$

$$\overline{\omega}_T = \overline{\rho}_u \frac{1}{\tau_K} \overline{c}(1-\overline{c}) f_W \quad \cdots\cdots(2a)$$

$$\overline{\omega}_L = \overline{\rho}_u S_t \left|\nabla \overline{c}\right| \quad \cdots\cdots(2b)$$

where c is the progress variable, S_t the turbulent burning velocity, τ_K the Kolmogorov time scale, and ρ_u the density of the unburned gas; f_W denotes a model function for the wall effect, which is described in a later section; the symbol over bar $\overline{\ }$ indicates ensemble averaged quantity or mean quantity.

The mass of fuel consumption per unit time and volume, $\overline{R}_{fu}$, is given by

$$\overline{R}_{fu} = C_{\mathrm{model}}\, \overline{\omega}(y_{fu,u} - \overline{y}_{fu,b}) \quad \cdots\cdots(3)$$

where C_{model} is a model constant, $y_{fu,u}$ the fuel mass fraction in an unburned mixture and $y_{fu,b}$ the fuel mass fraction in the burned gas. As the relationship between the most energetic length scale, ℓ, and the integral length scale ℓ_I is vague quantitatively, ℓ is assumed ℓ_I for the present study.

TURBULENT DISSIPATION FLAMELET

The equations for the fractal dimension D_T and Kolmogorov time scale τ_K in Eq. (1) are derived from the turbulence energy spectrum function and the relationships between the turbulence variables averaged over a three-dimensional space and those averaged over a D_T -dimensional space. The details of the formulation are shown in Ref. (3) and only the final formulae are shown below,

$$D_T = D_T^{\,*} F_D \quad \cdots\cdots(4)$$

$$D_T^{\,*} = 5 - 1.03\alpha^*(1 + 5.30 R_t^{-1/2}),\ \alpha^* = 2.27 \quad \cdots\cdots(4a)$$

$$F_D = 1 + \frac{1}{2.61 R_t^{\,0.276} - 5} \quad \cdots\cdots(4b)$$

$$R_t = \frac{k^2}{\varepsilon \nu} \quad \cdots\cdots(4c)$$

where k is the turbulent kinetic energy, ε its dissipation rate and ν the kinematic viscosity.

$$\frac{1}{\tau_K} = \left(\frac{\varepsilon}{\nu}\right)^{1/2} \left(\frac{\ell_K}{\ell}\right)^{(3-D_T)/2} \quad \cdots\cdots(5)$$

$$\frac{\ell_K}{\ell} = L^* F_L \quad \cdots\cdots(6)$$

$$L^* = \left\{ \frac{6\alpha^*}{(1+D_T)} \frac{1}{C'^{4/3} R_t} \right\}^{3/(1+D_T)} \quad \cdots\cdots(6a)$$

$$F_L = \frac{0.199 R_t^{\,0.805} - 2.19}{0.199 R_t^{\,0.805} - 1.19} \quad \cdots\cdots(6b)$$

$$C' = 0.201\left(1 + 5.30 R_t^{-1/2}\right)^{3/2} \quad \cdots\cdots(6c)$$

LAMINAR FLAMELET

The burning rate due to laminar flamelet is formulated on the basis of the fractal flame concept with the fractal dimension of laminar flame wrinkling, D_L. The ratio of a turbulent flame speed S_t to laminar flame speed S_ℓ is expressed in the following form:

$$\frac{S_t}{S_\ell} = \left(\frac{\varepsilon_i}{\varepsilon_o}\right)^{2-D_L} \quad \cdots\cdots(7)$$

where ε_o and ε_i are the outer cutoff and inner cutoff, respectively. The outer cutoff ε_o is taken to be ℓ for the present purpose and the inner cutoff ε_i is given by the empirical expression as a function of Karlovitz number presented by Gülder et al.[4]. Equation (7) is reduced to the form as,

$$\frac{S_t}{S_\ell} = \left(3.21 C_i C'^{1/4} \frac{\ell_K}{\ell}\right)^{2-D_L} \quad \cdots\cdots(8)$$

where C_i=2.5. The laminar flame speed S_ℓ is given by the empirical equation presented by Metghalchi et al.[5].

The fractal dimension D_L for the laminar flamelet is solved by the empirical differential equation, called Fractal Dimension Growth Model, that was developed by Suzuki et. al.[6], and described briefly in the following section.

FRACTAL DIMENSION GROWTH MODEL (FDGM)

It is a well-known experimental evidence that the turbulent flame structure of SI engine combustion grows as the flame propagates during an early phase following spark ignition. To express this nature, several models[7, 8, 9, 10] have been proposed for reducing the burning rate during the early phase of flame propagation. These models were constructed with respect to theoretical or phenomenological considerations, not from measurements of the turbulent flame structure itself. Suzuki et al.[6] measured the fractal dimension of the flame during an early phase of flame propagation in an optical SI engine

varying engine speeds and compression ratios, and indicated that the fractal dimension grows as the flame propagates. Upon analysing the data, they derived an empirical equation for the growth rate of the fractal dimension, which was expressed as a function of turbulence intensity and pressure, as shown below,

$$\frac{dD_2}{dt} = -\frac{1}{\tau}\{D_2 - D_{2\infty}\} \qquad \cdots\cdots(9)$$

$$D_{2\infty} = D_{2T} - (D_{2T} - 1.0)\exp\left[-c_0\left(\frac{\bar{p}}{p_0}\right)^{\gamma}\frac{u'}{S_\ell}\right]$$

$$D_{2t} = 1.32,\ c_0 = 0.13,\ \gamma = 0.72 \qquad \cdots\cdots(9a)$$

$$\tau = \tau_{C0}\left(\frac{\bar{p}}{p_0}\right)^{\phi}\left(\frac{u'}{S_\ell}\right)^{\zeta}$$

$$\tau_{C0} = 5.80\,[\text{ms}],\quad \phi = -0.34,\quad \zeta = -0.93 \qquad \cdots\cdots(9b)$$

where, D_2 is the fractal dimension of a flame cross section curve, p the pressure, p_0 the atmospheric pressure and u' the turbulence intensity. The fractal dimension D_L of a flame surface is obtained from the relationship $D_L = D_2 + 1$.

WALL EFFECT f_W

The function f_W in Eq. (2a) is to take into account a decrease in probability of burned and unburned gasblobs meeting each other in the turbulent dissipation flamelet regime in near wall regions. The wall effect function f_W is expressed in the form as[11],

$$f_w = \left(\frac{\ell_I}{C_\ell \ell_T}\right)^2 \quad , \quad \frac{1}{C_\ell^{\,2}} \le f_w \le 1 \qquad \cdots\cdots(10)$$

$$\frac{\ell_I}{\ell_T} = \left(\frac{C_\mu}{15}\right)^{1/2}\left(\frac{2}{3}\right)^{1/4} R_t^{\,1/2} \qquad \cdots\cdots(10a)$$

where ℓ_I is the integral length scale, ℓ_T the Taylor micro scale, $C_\mu = 0.09$, and C_ℓ is a model constant, which is set to 2.0 in the present study.

OUTLINE OF GOVERNING EQUATIONS

Governing equations to be solved are the general conservation equations in the Reynolds averaged form for mass, momentum, average enthalpy (over unburned and burned gases), enthalpy of unburned gas[3], progress variable, the turbulence kinetic energy and its dissipation rate. The standard k-ε model was employed for the turbulence model. The law of the wall for momentum and enthalpy gave the wall boundary conditions.

TEST ENGINE AND COMPUTATIONAL CONDITIONS

Two different four-stroke single cylinder engines were used for the computations and experiments. Each of them had a disk-shaped combustion chamber and a spark plug was located at the center of the cylinder head. They are named Engine A and Engine B in the text, and their specifications and test conditions are shown in Table 1. Engine A was used for the measurements varying engine speed and Engine B for the data varying the excess air ratio.

The computations were performed solving a set of the governing equations in an axisymmetric field. The mass fractions of residual gas were set to 0.13 and 0.1 for Engine A and Engine B, respectively, estimated by the one-zone global model. The pressure and temperature at the inlet valve closing were assumed for each test condition based on the experiments. The wall temperatures were set to 433 K for both engines given by measurements. The initial value of turbulence kinetic energy was assumed to be 0.74 $C_m^{\,2}$ (C_m: mean piston speed).

COMPUTATIONAL RESULTS AND COMPARISON WITH MEASUREMENTS

Engine A - In Fig. 1 shown are the measured pressures and the apparent heat release rates for Engine A operating at 1000, 1500 and 1800 rpm under excess air ratio λ=1.0. The apparent heat release rate was calculated from the pressure data assuming the ratio of specific heats to be 1.4. The laminar flamelet model for the wrinkled flame, which is made up of FDGM only, also was tested to see the difference from the HFFM. This model is expressed by setting $\gamma_K = 0$ in Eq. (2). The model constant C_{model} in Eq. (3) of each model was adjusted so as to obtain the best fit to the measured pressure for 1000 rpm. The model constants adjusted were 2.95, and 2.60 for the HFFM and the FDGM (or laminar flamelet model), respectively. Then the computations for 1500 rpm and 1800 rpm were performed using the same value of C_{model} for each model.

Table 1 Engine specifications and test conditions

[Engine A]		
Bore x Stroke	: 86.0 x 84.0 mm	
Comp. Ratio	: 7.9	
Fuel	: Regular gasoline	
Engine speed	Excess air ratio	Ign. time
1000 rpm	1.05	13 ° btdc
1500	0.997	14
1800	0.957	20
[Engine B]		
Bore x Stroke	: 82.6 x 114.3 mm	
Comp. Ratio	: 7.0	
Fuel	: Iso-octane	
Engine speed	Excess air ratio	Ign. Time
750 rpm	1.0	15 ° btdc
750	1.1	16
750	1.2	19

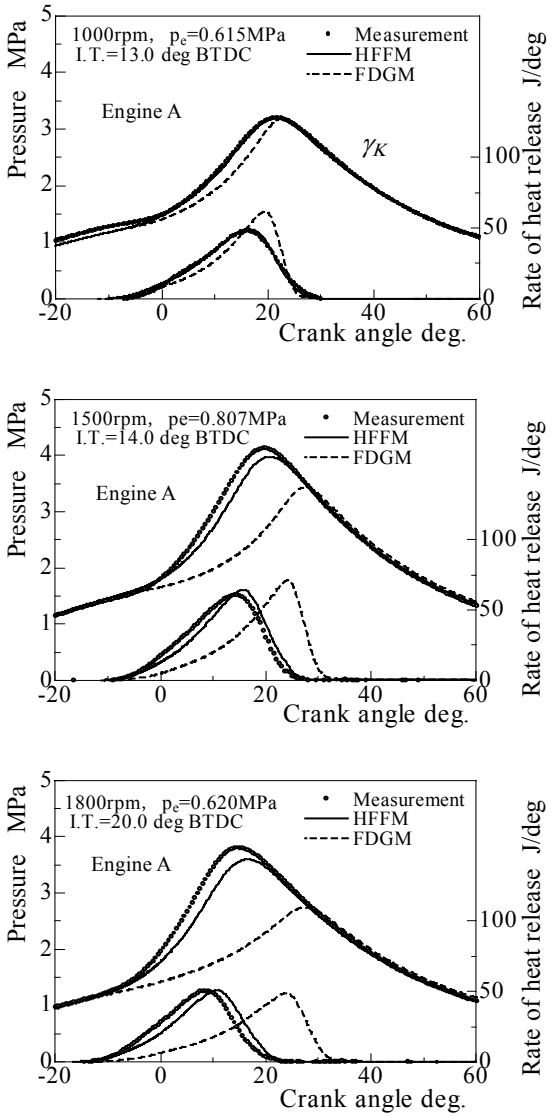

Fig. 1 Comparison of computational results by two different models with measurements for 1000, 1500 and 1800 rpm; Engine A; excess air ratio λ=1.0; C_{model}=2.95 for HFFM, C_{model}=2.60 for FDGM

The computed apparent heat release rate also was obtained from the pressure data assuming the ratio of the specific heats to be 1.4. It is seen that the HFFM gives much better results than the FDGM, which are very slow in combustion at 1500 and 1800 rpm.

Figure 2 indicates γ_K and the ratio of the turbulent dissipation heat release rate to the total heat release rate $R_{\omega T}$ as a function of crank angle. It is seen that γ_K is only 13% to 17%, being nearly independent of engine speed. In contrast, the turbulent dissipation heat release rate occupies a larger part as the engine speed increases from around 20% at 1000 rpm to 50% at 1800 rpm. This is mainly due to the fact that the Kolmogorov time scale τ_K becomes smaller as the turbulence increases, as shown in Fig. 3. It may be said that at 1000 rpm the role of the turbulent dissipation heat release rate is not considerable,

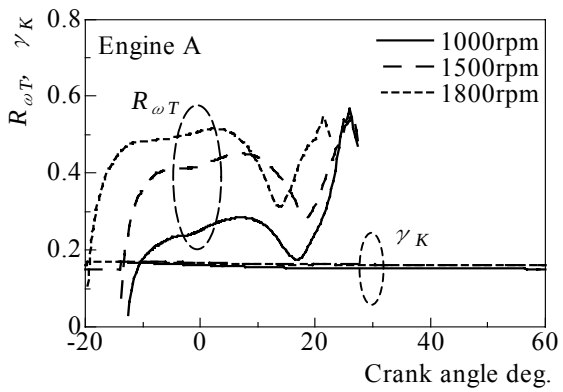

Fig. 2 Contribution of Turbulent dissipation flamelet; HFFM ; Engine A, $R_{\omega T} = \omega_T\gamma_k /[\omega_T\gamma_K + \omega_L(1-\gamma_K)]$

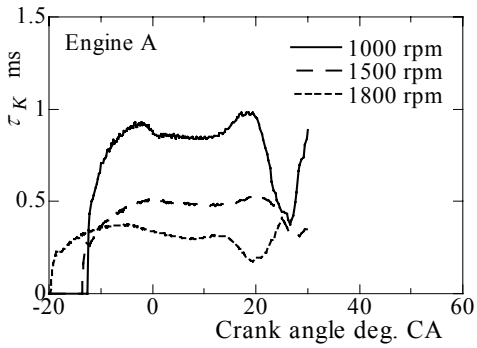

Fig. 3 Kolmogorov time scale averaged over flame region; HFFM, Engine A

while at 1800 rpm it is as large as half the total heat release rate.

Engine B - Figure 4 compares the computed pressure and heat release rate with the measurements for three different excess air ratios, 1.0, 1.1 and 1.2, at 750 rpm. The models taken for comparison with measurements are the HFFM, and the FDGM. The model coefficient C_{model} in Eq. (3) of each model was adjusted so as to fit the pressure for excess air ratio λ =1.0, and the same value was used for the other two different excess air ratios.

It is seen that for λ=1.1 both the HFFM and FDGM coincide well with the measurements. In the case of λ=1.2, the FDGM gives the better result than the HFFM, which overestimates a little.

Figure 5 shows the contribution of the turbulent dissipation flamelet for Engine B at λ=1.0. The value of γ_k is nearly the same as that for Engine A, while $R_{\omega T}$ is less than 16%, even less than that for Engine A at 1000 rpm. A general tendency seen in Figs. 2 and 5 is that the combustion relies on turbulent-dissipation more as engine speed increases and, vice versa, that it approaches the laminar flamelet combustion as engine speed decreases.

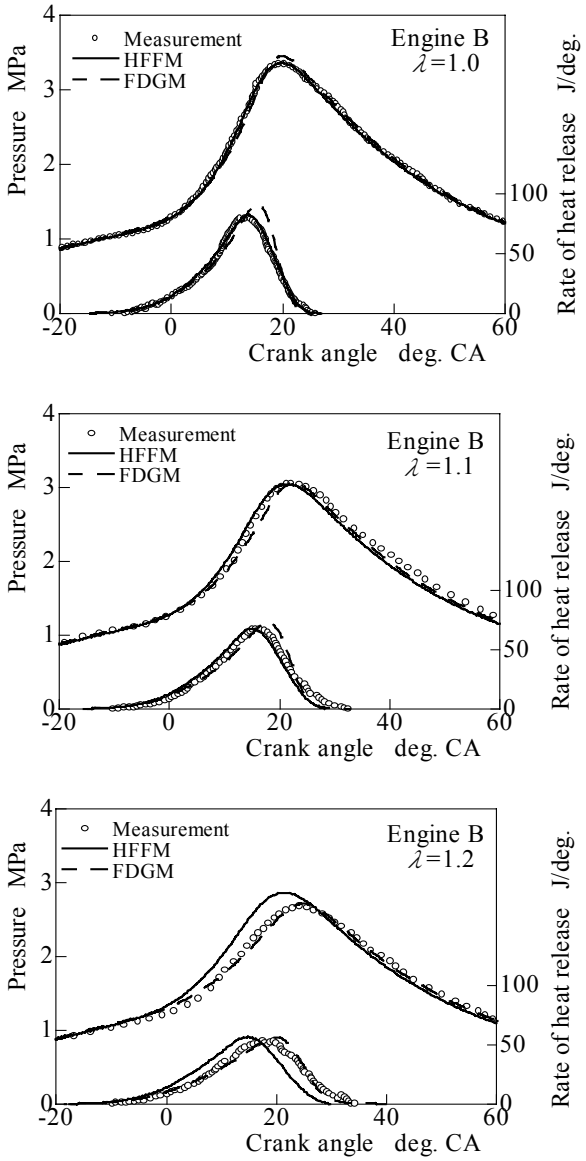

Fig. 4 Comparison of computational results by three different models with measurements for equivalence ratio λ = 1.0, 1.1 and 1.2;
Engine B, 750 rpm, C_{model}=1.65

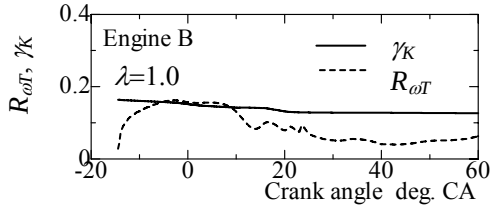

Fig. 5 Contribution of Turbulent dissipation flamelet; HFFM ; Engine B, λ=1.0
$R_{\omega T} = \omega_T\gamma_k / [\omega_T\gamma_K + \omega_L(1-\gamma_K)]$

CONCLUSION

A new combustion model, Hybrid Fractal Flame Model, has been introduced for the turbulent propagating flame in an SI engine. The model is formulated by the concept that the flame front consists of the laminar mixing flamelet and turbulent dissipation flamelet. The computed results were compared with measured pressures for several different excess air ratios and engine speeds. From the comparison of the computed results with the measurements and the analysis of the computed results, the following conclusions are drawn from this study.

(1) The Hybrid Fractal Flame Model, which combines the turbulence dissipation model and the Fractal Dimension Growth Model, predicts well the measured pressures as a whole for different conditions tested in this study.
(2) The laminar flamelet model tends to delay in combustion as engine speed increases.
(3) The analysis of the computed results shows that the turbulence dissipation heat release rate occupies more in the total heat release rate as engine speed increases.

ACKNOWLEDGEMENT

The authors would like to thank Dr. K. Saijyo (currently, Isuzu Advanced Engineering Center, Ltd.) for making the CFD code and for the discussion with the authors on the combustion models when he studied at Ritsumeikan University. Thanks are also due to Dr. K. Suzuki (currently, Hitachi, Ltd.) for developing the Fractal Dimension Growth Model and to Mr. Minoura (currently, Suzuki Motor Co.) for modifying the CFD code when they studied at Ritsumeikan University.

REFERENCES

(1) Gülder, O. et al., "Flame Front Surface Characteristics Turbulent Premixed Propane/Air Combustion," Combustion and Flame, Vol. 120, pp. 407-416, 2000.
(2) Smallwood, G. J., "Flame Surface Density Measurements with PLIF in an SI Engine," SAE Paper No. 962088, 1996.
(3) Nishiwaki, K., "Modeling Engine Heat Transfer and Flame-Wall Interaction," Proc. COMODIA 98, pp. 35-44, 1998.
(4) Gülder, O. L. and Smallwood, G. J., Combustion and Flame, Vol. 103, pp.107-114, 1995.
(5) Metghalchi, M. and Keck, J. C., "Burning velocities of Mixtures of Air with Methanol, Isooctane, and Indolen at High Pressure and Temperature," Combustion and Flame, Vol. 48, p.191-210, 1982.
(6) Suzuki, K. and Nishiwaki, K., "Fractal Dimension Growth Model for SI Engine Combustion," SAE 2004-01-1993, 2004.
(7) Weller, H. G., Uslu, S., Gosman, A.D., Maly, R. R., Herweg, R. and Heel, B., "Prediction of Combustion in Homogeneous-Charge Spark-Ignition Engines," Proc. COMODIA94, pp. 163-169, 1994.
(8) Zhao, X., Matthews, R. D. and Ellzey, J. D, "Numerical Simulation of Combustion in SI Engines: Comparison of the Fractal Flame Model to the Coherent Flame Model," Proc. COMODIA 94, pp. 157-162, 1994.

(9) Herweg, R. and Maly, R. R.," A Fundamental Model for Flame Kernel Formation in S. I. Engines," SAE Paper 922243, 1992.
(10) Santavicca, D. A., Liou, D. and North, G. L., "A Fractal Model of Turbulent Flame Kernel Growth," SAE Paper 900024, 1990.
(11) Kojima, K. and Nishiwaki, K., "Modeling of flame-wall interaction for combustion and heat transfer in S.I. engines," JSAE Review Vol. 18, pp. 11-17, 1997.

29th IEA-TLM, Gembloux, Belgium, 3-5, September, 2007
3.1D: Analysis of Turbulent Combustion Flows

Molecular Velocimetry Using Photothermal Grating Induced by Laser-Multibeam Interference

Noboru Nakatani

Department of Business Administration Education,
Ashiya University□13-22, Rokurokuso-cho, Ashiya,
Hyogo 659-8511, Japan□nakatani@ashiya-u.ac.jp

Abstract

This paper describes the tagging velocimetry system for measuring the velocity distributions on multiline using photothermal grating. Firstly, the grating is induced by multibeam interference to make the grating image sharp. The sharp grating reduces the influence of molecular diffusion, which is inherent problem in molecular velocimetry. Secondly, the gratings of wide interval are induced by the use of diffraction gratings without and with modulation, to measure velocity in wide range. To detect the change of refractive index by the photothermal effect, we used the CCD-LD differential interferometer, which was developed in our previous study. The interferometer has functions of spatial and temporal differentiation for reducing the influence of phase fluctuations due to turbulent mixing.

1. Introduction

Particle Image Velocimetry (PIV)], [Adrian (1991)] and Doppler Gloval Velocimetry (DGV), [Meyer (1995)] have been developed for the measurement of flow velocity distributions. However, these methods need to seed scattering particles in flow. This is not desirable in many testing environments. For example, the seed particles do not faithfully reproduce the gas flow in high speed. Especially, in flow diagnostics indoors it is desirable to keep the field clean for the health. These reasons have provided ample motivation for investigating unseeded molecular velocimetry methods. Several molecular-based methods have been developed to alleviate the problems associated with seeding flow. In practice, many of these methods exhibit a new set of drawbacks. For example, Doppler-based methods suffer

from poor dynamic range and yield large measurement in lower velocity limits [Miles and Lempert (1990)]. Ozone tagging velocimetry using photodissociation needs to take 20 μs for induction of the ozone [DeBarver, Rivarver, Wehrmeyer, Batiwata, and Pitz (1998)]. To be freed from these problems, molecular velocimeter using photothermal effect have been investigated [Nie, Hane and Gupta (1986)] and [Nakatani (1994), (2000), (2002)]. In the velocimeters velocity distributions are measured point by point. In our previous study we developed the tagging velocimetry for the velocity distributions of gas flow on one line using the photothermal effect. [Nakatani (1998)].

This paper describes the tagging velocimetry system for measuring the velocity distributions on multiline using photothermal grating. Firstly, the grating is induced by multibeam interference to make the grating image sharp. The sharp grating reduces the influence of molecular diffusion, which is inherent problem in molecular velocimetry. Secondly, the gratings of wide interval are induced by the use of diffraction gratings without and with modulation [Nakatani et al.(1988)], to measure velocity in wide range. To detect the change of refractive index by the photothermal effect, we used the CCD-LD differential interferometer, which was developed in our previous study [Nakatani(1998)]. The interferometer has functions of spatial and temporal differentiation for reducing the influence of phase fluctuations due to turbulent mixing.

2. Measuring system

The schematic diagram of the tagging velocimetry system are shown in Fig. 1. A jet of a gas mixture of nitrogen and ethylene is used as a flow. A pump beam is irradiated to flow for producing a photothermal tagged line. The photothermal tagged line is conducted downstream and is observed by the differential interferometer at the time-of-flight delay. The difference in the phases between the measuring points is measured for obtaining the velocity distribution. The differential interferometer developed by smith (1955) is used for detecting phase change by photothermal effect. A laser diode of 635 nm in wavelength, 100 mW in power and single mode is used as a light source of double pulses. Because the laser diode is suitable to make short pulse light in high frequency. The phase difference at two points is detected. The laser beam is collimated by a lens L1. The polarization direction of the laser beam is rotated at angle of 45 degree to the optic axis of a Wollaston prism with a half wavelength plate HWP between the lens L1 in focal length of 100 mm and the flow field. After the laser beam passes through a flow field, the beam is focused into a Wollaston prism WP in dividing angle 2.5 mrad with a lens L2 in focal length 200 mm for dividing two beams. The pair beams are passed through an analyzer AN and are interfered on image plane. The phase difference at two points of objects separated by the distance 0.5 mm between the pair beams is detected. The operating point of the interferometer at a detector output signal is set

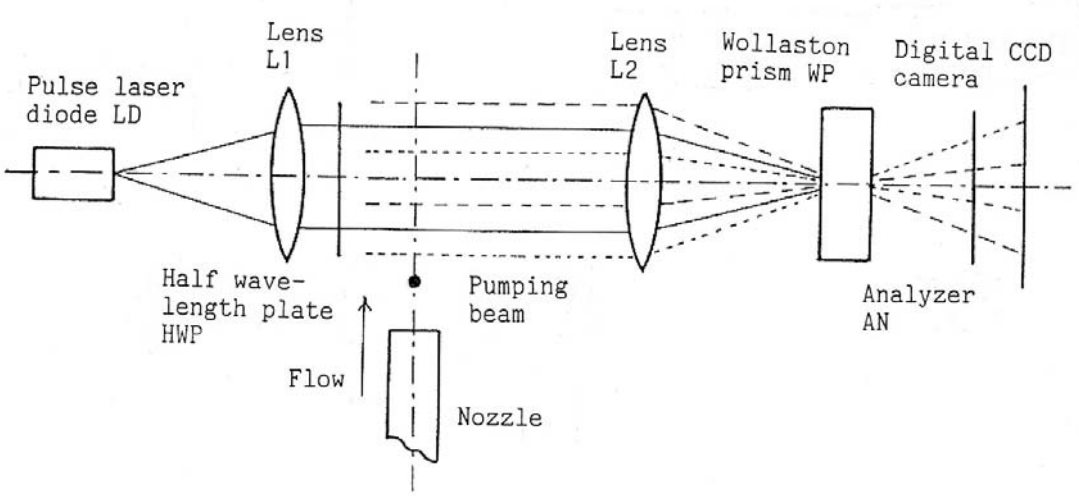

Fig. 1 The measurement system of flow velocity distribution using a differential interferometer.

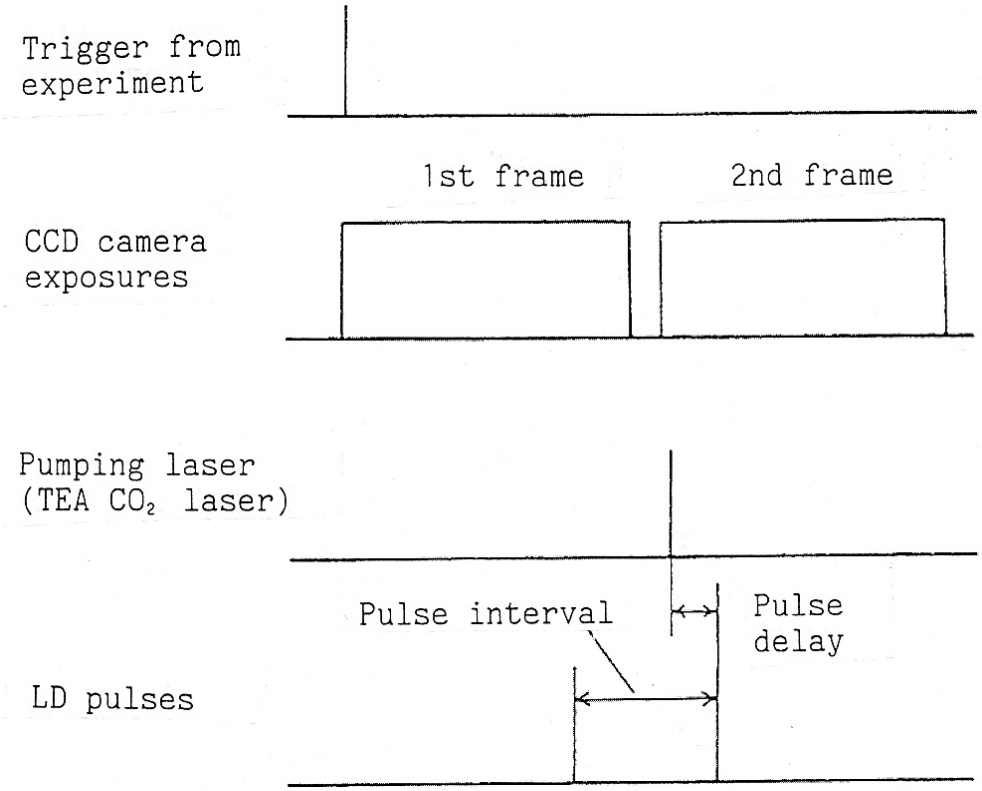

Fig. 2 The external synchronization of the CCD camera cycle with the pulses of a laser diode and the pumping pulse laser.

at the maximum inclination point of a fringe intensity curve by displacement of the Wollaston prism WP. To reduce the influence of phase fluctuation in turbulent flow, we use a digital CCD camera synchronization in association with double pulses of the laser diode for recording images of the differential interferometer. The interference images before pumping and after pumping are recorded, as shown in Fig. 2. The pulses of the laser diode LD are generated between closely two frames in a digital CCD camera, which has the same exposure function as that used in the PIV technique. To reduce the fluctuation of phase difference due to turbulence, optical distortion and noise, the images before pumping and after pumping are differentiated by the image processor.

3. Multibeam pumping system and experimental results

We use three beam interference for observing local field in high spatial resolution by inducing sharp photothermal grating. We used a multi slit system shown in Fig. 3. The length of the three rectangular slits used is 5 mm and the width 0.50 mm. The interval between slits is 2 mm. The slits are made by a stainless steal in thickness of 0.100 mm for enduring the energy of CO_2 laser. Three beam pumping using the slits is compared with two beam pumping. The intensity distribution of the photothermal grating detected by the differential interferometer system shown in Fig. 2 is shown in Figs. 4 and 5. The photothermal grating fringe induced by three beam interference is sharper than that by two beam interference.

Using jets of a 9:1 in volume mixture of nitrogen and ethylene, we confirmed that this measurement system using multibeam interference pumping is useful to measure the flow velocity distributions on multiline under turbulent phase fluctuation. A typical velocity distribution image obtained by three beam interference is shown in Fig. 6. This technique is useful to measure change of velocity gradients in a local field.

The photothermal gratings are induced by pumping by the use of diffraction gratings without and with modulation for observing wider field comparing with multibeam interference method. The grating without modulation is made by stainless steal of 0.100 mm in thickness for enduring the energy of CO_2 pulse laser. The width of the blank and transparent part in the rectangular slit is 0.25 mm, that of the filling and opaque part 0.25 mm, the length 10 mm, and the period 0.5 mm. The results of the demonstration using this diffraction grating are shown in Figs. 7 and 8. Fig. 7 shows the intensity distribution of photothermal grating observed by the differential interferometer. The ratio of intensity of 1st order to that of 0th order about 0.5. The period of the photothermal grating is 1.06 mm. The fringe is sharp by multiple interference pumping. In Fig. 8 we can see the slight transition of jet.

The diffraction grating with modulation is used for observing wider field compared with the method of the grating without modulation. The structure of the of the diffraction grating of a pulse width modulation is shown in Fig. 9. The intensity distribution of the photothermal grating induced by this modulation

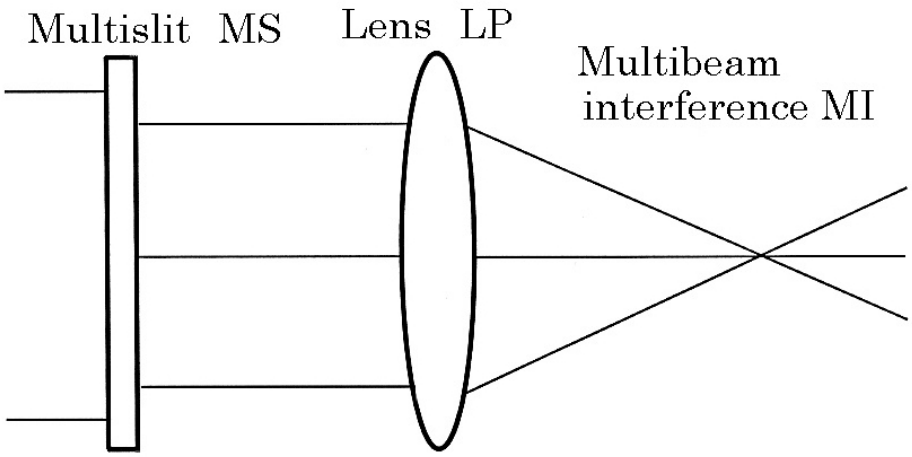

Fig. 3 Two or three focused pump beams by the use of slits of rectangular holes.

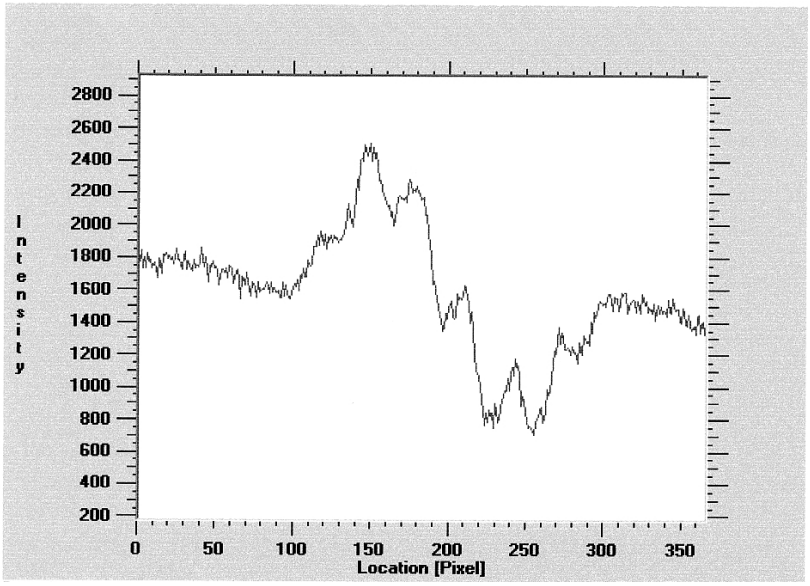

Fig. 4 Typical intensity distribution of photothermal grating. by two beam interference. Elapsed time after pumping 4μs.

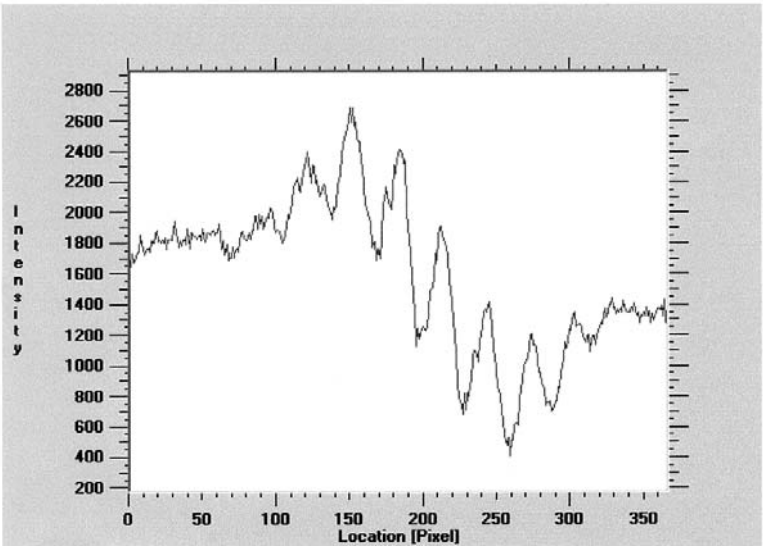

Fig. 5 Typical intensity distribution of photothermal grating. by three beam interference. Elapsed time after pumping 4μs.

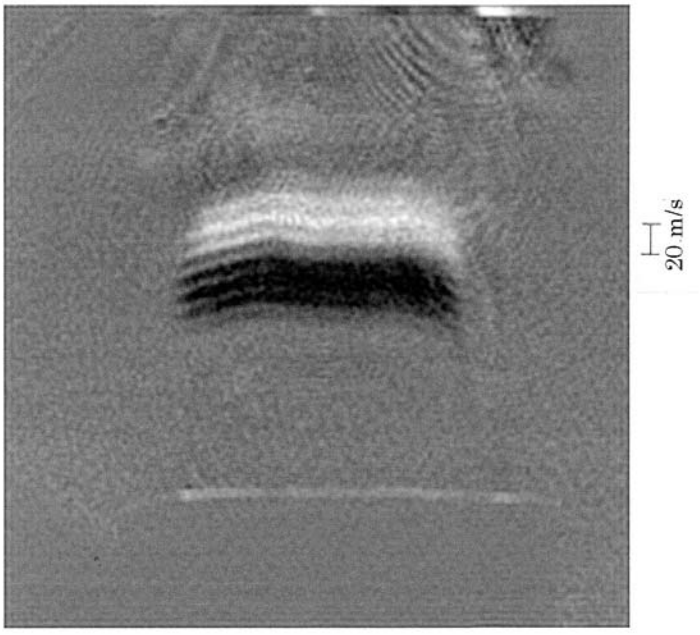

Fig. 6 Typical pattern of flow velocity distributions on multiline by three beam interference.

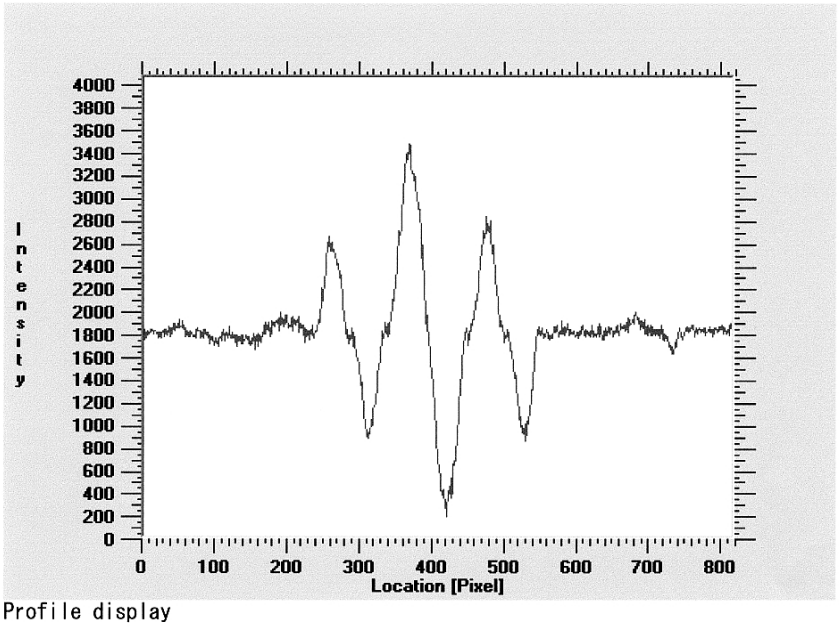

Fig. 7 Typical intensity distribution of photothermal grating by the use of the diffraction grating without modulation. Elapsed time after pumping 29 μs.

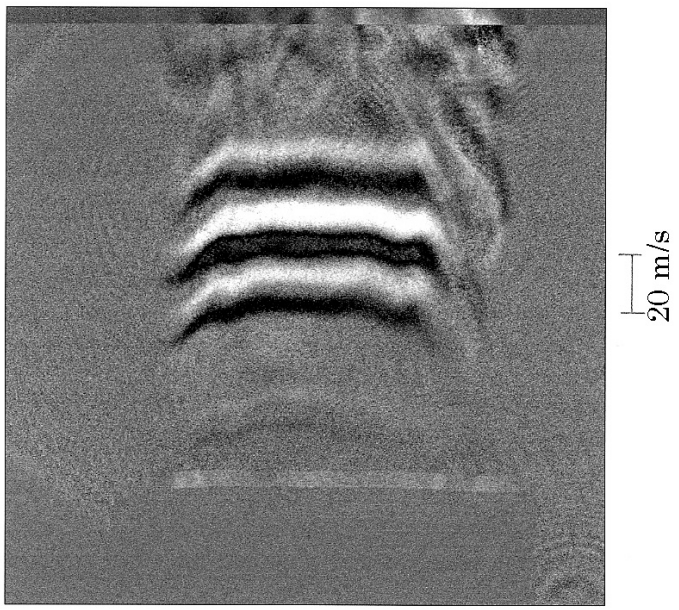

Fig. 8 Typical pattern of flow velocity distributions on three lines by the use of diffraction grating without modulation.

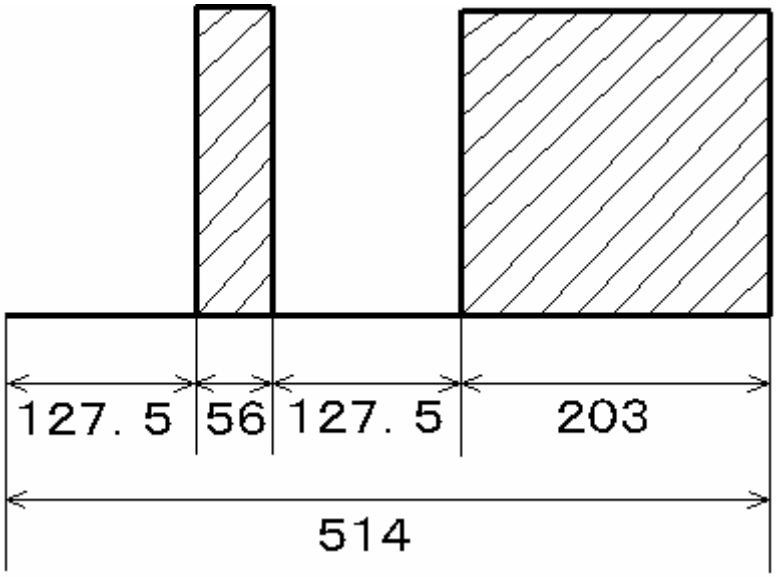

Fig. 9 Structure of the diffraction grating with pulse width modulation for 5-7 lines photothermal grating. Unit is μm.

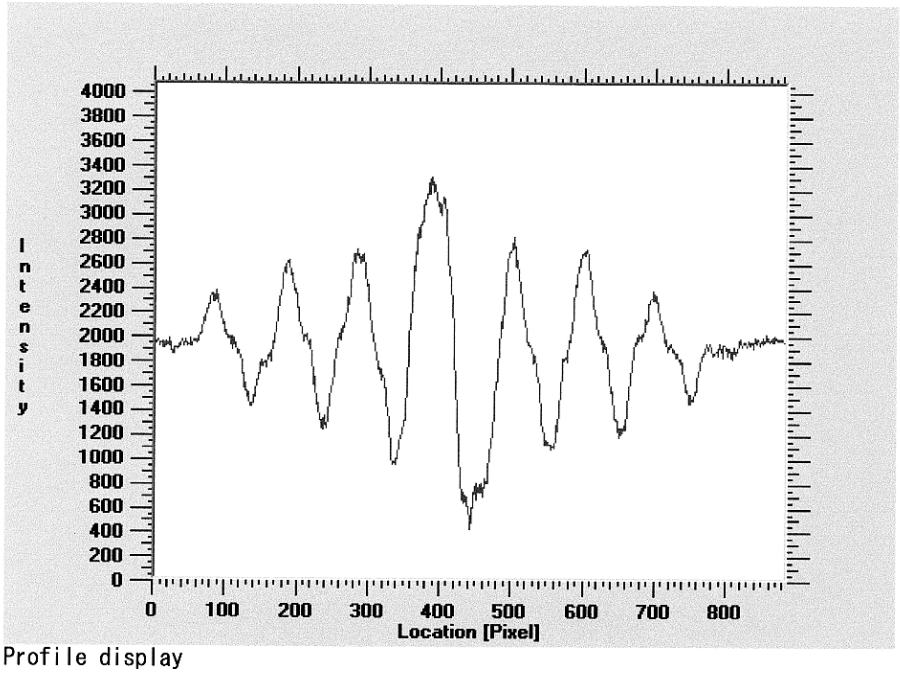

Fig. 10 Typical intensity distribution of photothermal grating by the use of the diffraction grating with pulse width modulation, Elapsed time after pumping 29μs

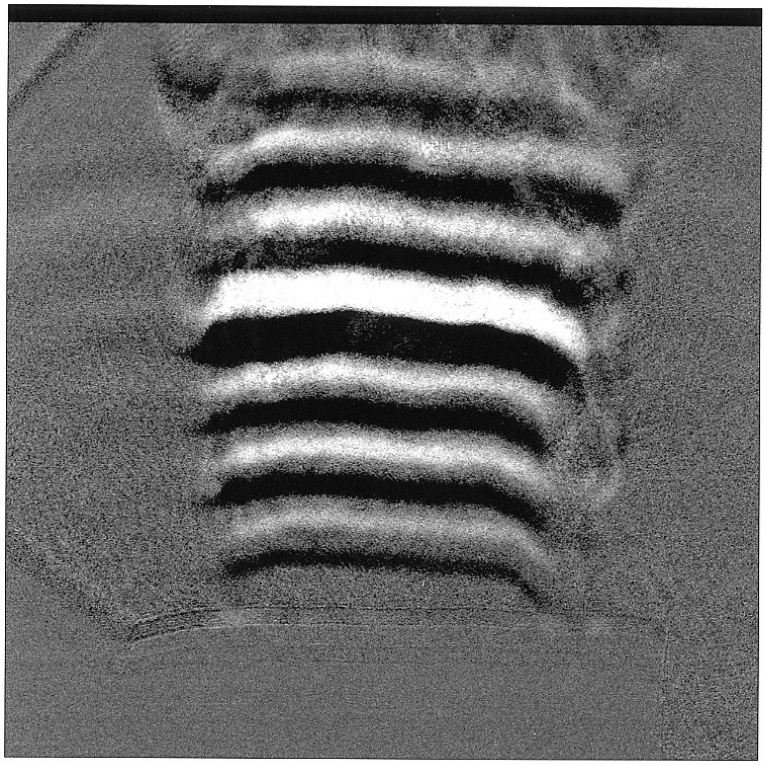

Fig. 11 Typical pattern of flow velocity distributions on seven lines by the use of the diffraction grating with the pulse width modulation.

diffraction grating is shown in Fig. 10. The period of the photothermal grating is 1.03 mm. We can observe flow velocity distribution on 7 lines by photothermal grating. The result of the demonstration using this diffraction grating is shown in Fig. 11. We can see the transition of jet in wide field. As we use the amplitude grating in this study, the intensity of 0th order diffraction beam is larger than that of higher order diffraction beam. To improve the intensity difference between each beam, we will report shortly the result by the use of a phase diffraction grating..

The diffraction gratings make it possible to induce photothermal grating of wide interval and 3 - 9 lines.

References

Adrian, R. J., (1991), Particle-imaging Technique for Experimental Fluid Mechanics, Ann. Rev. Fluid Mech. Vol. 23, pp.261 - 304.

Meyer, J. F., (1991), Development of Doppler Gloval Velocimetry as Flow Diagnostics Tool, Meas. Sci. Technol. Vol.6, pp.769 - 763.

DeBarver, P. A., Ribarov, L. A., Wehrmeyer, J. A., Batliwala, F.and Pitz, R. W., (1998), Quantitative Unseeded Molecular Velocimetry Imaging, Proc.

of the 9th Int. Symp. on Applications of Laser Techniques to Fluid Mechanics, Institute Superior Tecnico, pp.34-1-1 -32-1-6.
Miles, R. and Lempert, W., (1990), Two-Dimensional Measurement of Density, Velocity and Temperature in Turbulent High Speed Air Flows by UV Rayleigh Scattering, Appl. Phys. Vol. B51, pp.1 - 7.
Nakatani, N., Oshio, T., (1994), Measurements of Gas Flow Velocity and Temperature Using Laser Photothermal Effect with the Differential Interferometer, Proc. of the 7th Int. Symp. on Applications of Laser Techniques to Fluid Mechanics, Institute Superior Tecnico, pp.32-5-1 - 32-5-8.
Nakatani, N., (2000), Measurements of the Velocity and Temperature in a Turbulent Flow by the Laser Photothermal Effect with the New Compulsorily Phase Locked Interferometer, Rev. of Sci. Instrum, Vol. 71, No 5, pp.1971 - 1974.
Nakatani, N., (2000), Laser Photothermal Velocimeter with the Differential Interferometer Using Orthogonally Polarized Light Source of Modulated LD, Proc. of the 10th Int. Symp. on Applications of Laser Techniques to Fluid Mechanics, Institute Superior Tecnico, pp. 15-3-1 - 15-3-9.
Nakatani, N., (2002), Molecular Photothermal-Velocimeter of High Spatial Resolution by Partially Crossed Probing, Proc. of the 11th Int. Symp. on Applications of Laser Techniques to Fluid Mechanics, Institute Superior Tecnico, pp.30-1-1 - 30-1-9.
Nakatani, N., (1998), Measurement of the Velocity Distribution of turbulent Flow by the Laser Photothermal Effect with a CCD-LD-interferometer, Proc. of the 8th Int. Symp. on Applications of Laser Techniques to Fluid Mechanics, Institute Superior Tecnico, pp.34-6-1 - 34-6-8.
Nakatani et al, (1988), Advancing Multipoint Optical Fiber LDV's-Vorticity Measurement and Some New Optical Systems, Laser Anemometr in Fluid Mechanics 3, LADOAN, pp.3 - 18.
Nie, Y. X., Hane, K. and Gupta, R., (1986), Measurements of Very Low Gas Flow Velocities by Photothermal Deflection Spectroscopy, Appl. Opt. Vol. 25, pp. 3247 - 3252.